ACS OMEGA

http://pubs.acs.org/journal/acsodf

Article

Study on Pyrolysis of Shale Gas Oil-Based Drilling Cuttings: Kinetics, Process Parameters, and Product Yield

Pu Liu, Quanlin Xiao,* Ning Dai, Zhongbin Liu, and Chenlong Wang

Cite This: *ACS Omega* 2023, 8, 13593−13604

Read Online

ACCESS | Metrics & More | Article Recommendations

ABSTRACT: The main reaction range (350−550 °C) of oil-based drilling cutting (OBDC) pyrolysis was studied by a thermogravimetric analyzer and a vacuum tube furnace. The average activation energies calculated by four model-free methods were 185.5 kJ/mol (FM), 184.16 kJ/mol (FWO), 166.17 kJ/mol (KAS), and 176.03 kJ/mol (Starink). The reaction mechanism was predicted by the Criado (Z-master plot) method. It is found that a high heating rate is helpful to predict the reaction mechanism, but it cannot be described by a single reaction model. Under the conditions of target temperature higher than 350 °C, residence time higher than 50 min, laying thickness less than 20 mm, and heating rate lower than 15 °C, the residual oil content is lower than 0.3% and the recovery rate of mineral oil is higher than 98.43%. Solid phase products accounted for more than 70%, reached the maximum 17.04% at 450 °C, and then decreased to 15.87% at 500 °C. Aromatic hydrocarbons, as coking precursors, are transformed from a low ring to a high ring. Recycled mineral oil can reconfigure oil-based mud (OBM). The research results can provide a theoretical basis for process optimization.

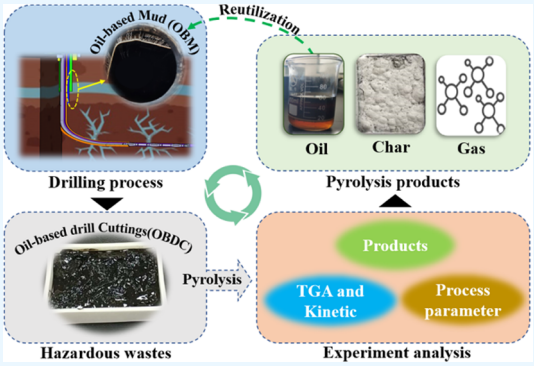

1. INTRODUCTION

As an important new energy source in the world, shale gas has achieved commercial development in China. In 2020, China's total shale gas production was 200 × 10^8 m^3, ranking second in the world.[1] However, oil-based mud (OBM) is required in shale gas exploration and development. This in turn produces a large amount of oil-based cuttings (OBDCs) (the annual output of OBDCs in the Fuling shale gas region in Chongqing alone has reached 4 million tons[2]), which contain petroleum hydrocarbons, heavy metals, and alkaline salt. Improper disposal will pose a serious threat to the ecological environment and the safety of residents.[3−6] Therefore, OBDCs have been included in China's National Hazardous Waste List in 2021[7] and are strictly controlled.

There are many methods for the treatment and resource utilization of OBDCs, including composting, microwave heating, solvent extraction, and copyrolysis.[5,8−10] However, due to the low processing efficiency, complex process, high cost, low crude oil recovery rate, and the possibility of secondary pollution, it has not been developed commercially. Pyrolysis treatment of OBDCs has the advantages of good treatment effect, significant harmlessness, high resource utilization, less air pollution, and stable operation and has been widely used in southern Sichuan, China.[4,11] However, there are few studies on the kinetic parameters and reaction mechanism of OBDCs.

The evaluation of kinetic parameters and the pyrolysis reaction mechanism are critical for optimizing process parameters, expanding the production scale, and designing pyrolysis reaction systems.[12] Methods developed by thermogravimetric analysis (TGA) are best suited to study the pyrolysis process of various sludges.[13,14] OBDCs have various components, the pyrolysis process is complex and changeable, and the activation energy changes significantly throughout the process. The model-free method (iso-transformation method) is usually used to estimate kinetic parameters such as activation energy, and its biggest advantage is that there is no risk of choosing the wrong dynamic model and finding unreasonable dynamic parameters.[15] Commonly used model-free methods are the Flynn−Wall−Ozawa (FWO) method, the Kissinger−Akahira−Sunose (KAS) method, and the Starink and Friedman (FM) method. The Z-master plot (Criado) method can be used to predict the reaction mechanism of complex raw materials, and the most suitable reaction mechanism model can be obtained by comparing the assumed kinetic model with the experimental data.[16,17] Although many researchers have studied the kinetics, thermodynamic parameters, and reaction mechanisms of pyrolysis processes such as oil sludge, sludge,

Received: November 17, 2022
Accepted: March 27, 2023
Published: April 4, 2023

and coconut shells, few studies have been reported on the pyrolysis of OBDCs.[18−20]

Similarly, the parameters of the solution process are also very important for the pyrolysis effect of OBDCs. Optimizing pyrolysis process parameters can improve the recovery rate of oil substances and reduce the oil content in oil-based ash. At the same time, it reduces the difficulty of the cement kiln coprocessing process, and the recovered oil material can also be reused. The standard for evaluating the effect of resource utilization is the amount of recovered pyrolysis oil, that is, the yield of mineral oil (m_o). The pyrolysis of OBDCs is usually divided into low-temperature pyrolysis (LTTD), high-temperature pyrolysis, and medium-temperature pyrolysis.[4] Generally, the pyrolysis reactors include spiral, rotary kiln, and hot distillation furnace reactors, and the pyrolysis effect also depends on the suitability of the raw materials and the reactor.[21]

This study is based on hazardous waste (OBDC) for thermogravimetric analysis and pyrolysis research. Four model-free methods (FWO, KAS, Starink, and FM) were used to calculate the activation energy and predict the reaction mechanism by the Z-master plot method. In addition, pyrolysis experiments were carried out in a vacuum tube pyrolysis furnace to study the effects of pyrolysis final temperature (target temperature T_g), residence time (t_i), heating rate (T_i), and laying thickness (h_i) on the product yield. This study can provide theoretical and data support for the pyrolysis technology of OBDCs.

2. MATERIALS AND METHODS

2.1. Materials and Characterization. The OBDCs used in this study were obtained from a shale gas exploration well in a block in southern Sichuan, China. In order to ensure the accuracy of OBDC measurement, three OBDCs were measured and the average value was obtained. The pH value was determined by the "Corrosion Determination of Solid Waste Glass Electrode Method".[22] The water content was measured by the distillation method, the slag content was measured by "Industrial Analysis of Coal",[23] and the oil content was measured by Soxhlet extraction-infrared spectrophotometry. Determination of the content of C and H was done using an organic element analyzer (Vario EL III, Elemeraor Company, Germany); determination of the S content was done according to the Ehrlich method of "Determination of Total Sulfur in Coal" (GB/T 214-2007); and according to the "Method for Determination of Chlorine in Coal" (GB/T 3558-2014), the Cl content in waste OBDC was determined by the Eschka-mixture fusion sample-potassium thiocyanate titration method. Through constant volume treatment, heavy metal elements were determined by ICP-AES. The measurement results are shown in Table 1.

2.2. Thermogravimetric Experiment. Pyrolysis was carried out using the American TA-SDTQ600 synchronous thermal analyzer. The OBDC samples were placed in an alumina crucible and heated from 30 to 900 °C at three heating rates of 10, 20, and 50 °C/min. The process maintained a nitrogen atmosphere with a gas flow rate of 50 mL/min. After the data recorded by the thermogravimetric analyzer was obtained, the next step was analyzed. Each experiment was performed twice to reduce experimental error.

2.3. Kinetic Study. *2.3.1. Kinetic Theory.* Due to the complex composition of waste OBDCs, it is difficult to describe the entire reaction process through one or several reactions during the pyrolysis process. Therefore, it is impossible to predict the exact reaction mechanism. Generally, the solid-state reaction of general solid waste pyrolysis can be described by the following formula[13]

$$\text{solid fuel (OBDC)} \xrightarrow{K(T)} \text{volatiles (condensable + noncondensable) + char} \quad (1)$$

According to the Arrhenius equation, the reaction rate constant (k) is defined as

$$k = A e^{-(E/RT)} \quad (2)$$

where A is the pre-exponential factor, min^{-1}; E is the reaction activation energy, J/mol; R is the molar gas constant, 8.314 J/(mol·K); and T is the thermodynamic temperature, K.

The polynomial reaction rates ($d\alpha/dt$) of solid fuels during pyrolysis can be defined as follows

$$\frac{d\alpha}{dt} = k(T) f(\alpha) \quad (3)$$

where k is the reaction rate constant, T is the absolute temperature, $f(\alpha)$ is the reaction mechanism function, and α is the conversion rate, defined by the following formula

$$\alpha = \frac{m_0 - m_t}{m_0 - m_f} \quad (4)$$

where m_0 is the initial mass of the reactant, g; m_t is the real-time mass of the reactant during the reaction, g; and m_f is the remaining mass after the reaction, g.

By combining eqs 2 and 3, we get that the reaction rate equation can be written as

$$\frac{d\alpha}{dt} = A e^{-(E/RT)} f(\alpha) \quad (5)$$

In thermogravimetric analysis, the heating rate constant value can be expressed as

$$\beta = \frac{dT}{dt} \quad (6)$$

Temperature and heating rate influence each other in thermogravimetric experiments, and formula 6 can be expressed as the temperature derivative.[16] Therefore

$$\frac{d\alpha}{dT} = \frac{d\alpha}{dt}\frac{dt}{dT} \quad (7)$$

Table 1. Basic Characteristics of OBDC

properties	OBDC	properties	OBDC
physicochemical composition (wet basis)	mean, %	metal elements (dry basis)	mass (wt %)
pH	8.83	Al	1.70
moisture	8.28	Si	9.50
oil	18.35	Mg	0.37
ash	73.37	Fe	1.20
nonmetallic elements (dry basis)	mass (wt %)	Ca	4.30
C	14.33	K	0.67
H	1.94	Sr	0.51
S	5.60	Ba	24.30
Cl	0.33	Na	0.34
		Ti	0.11

https://doi.org/10.1021/acsomega.2c07379
ACS Omega 2023, 8, 13593−13604

Table 2. Different Kinetic Models for Solid-State Kinetics[24]

reaction model	code	$f(\alpha)$	$g(\alpha) = \left(\int_0^\alpha \frac{d\alpha}{f(\alpha)}\right)$
		Diffusion Models	
one-dimensional diffusion	D1	$(2\alpha)^{-1}$	α^2
two-dimensional diffusion (Valensi model)	D2	$[-\ln(1-\alpha)]^{-1}$	$(1-\alpha)\ln(1-\alpha)+\alpha$
three-dimensional diffusion (Jander model)	D3	$\frac{3}{2}(1-\alpha)^{2/3}[1-(1-\alpha)^{1/3}]^{-1}$	$[1-(1-\alpha)^{1/3}]^2$
three-dimensional diffusion (Ginstling model)	D4	$\frac{3}{2}(1-\alpha)^{2/3}[1-(1-\alpha)^{1/3}]^{-1}$	$1-\frac{2\alpha}{3}-(1-\alpha)^{2/3}$
		Sigmoidal Rate Equations	
Prout−Tomkins	F1	$\alpha(1-\alpha)$	$-\ln(1-\alpha)$
		Geometrical Contraction Models	
contracting cylinder	F2	$2(1-\alpha)^{1/2}$	$1-(1-\alpha)^{1/2}$
contracting sphere	F3	$2(1-\alpha)^{2/3}$	$1-(1-\alpha)^{1/3}$
		Nucleation or Growth Models	
random nucleation (1)	F4	$(1-\alpha)^2$	$(1-\alpha)^{-1}$
random nucleation (2)	F5	$(1-\alpha)^3/2$	$2(1-\alpha)$
power law	P2/3	$\frac{2}{3}\alpha^{-1/2}$	$\alpha^{3/2}$
power law	P2	$2\alpha^{1/2}$	$\alpha^{1/2}$
power law	P3	$3\alpha^{2/3}$	$\alpha^{1/3}$
power law	P4	$4\alpha^{3/4}$	$\alpha^{1/4}$
Avrami−Erofeev	A1	$\frac{3}{2}(1-\alpha)[-\ln(1-\alpha)]^{1/3}$	$[-\ln(1-\alpha)]^{2/3}$
Avrami−Erofeev	A2	$2(1-\alpha)[-\ln(1-\alpha)]^{1/2}$	$[-\ln(1-\alpha)]^{1/2}$
Avrami−Erofeev	A3	$3(1-\alpha)[-\ln(1-\alpha)]^{2/3}$	$[-\ln(1-\alpha)]^{1/3}$
Avrami−Erofeev	A4	$4(1-\alpha)[-\ln(1-\alpha)]^{3/4}$	$[-\ln(1-\alpha)]^{1/4}$
		Order-Based Models	
first order	R1	$(1-\alpha)$	α^2
second order	R2	$(1-\alpha)^2$	$(1-\alpha)\ln(1-\alpha)$
third order	R3	$(1-\alpha)^3$	$[(1-\alpha)^{-2}-1]/2$
one and half order	R6	$(1-\alpha)^{3/2}$	$2[(1-\alpha)^{-1/2}-1]$

$$\frac{d\alpha}{dT} = \frac{d\alpha}{dt}\frac{1}{\beta} \tag{8}$$

Integrating eqs 5 and 8 yields the reaction rate equation

$$\frac{d\alpha}{dT} = \frac{A}{\beta}e^{-(E/RT)}f(\alpha) \tag{9}$$

It is given by integrating both sides of eq 9

$$g(\alpha) = \int_0^\alpha \frac{d\alpha}{f(\alpha)} = \frac{A}{\beta}\int_{T_0}^{T} e^{-(E_\alpha/RT)}\,dT \tag{10}$$

The $f(\alpha)$ and $g(\alpha)$ functional forms representing different reaction mechanisms are shown in Table 2. Equation 10, known as the integral form of the kinetic equation, describes the solid-state reaction mechanism during pyrolysis and requires an approximate solution using the iso-transformation model approach.

2.3.2. Model-Free Methods (Iso-Conversional Models). In this paper, the model-free methods used for kinetic analysis are Friedman, FWO, KAS, and Starink. Their mathematical expressions are as follows[25−27]

Friedman method (FR)

$$\ln\left[\beta_i\left(\frac{d\alpha}{dT}\right)_{\alpha,i}\right] = \ln[A_\alpha f(\alpha)] - \frac{E_\alpha}{RT_{\alpha,i}} \tag{11}$$

FWO method

$$\ln \beta_i = \ln\left[\frac{A_\alpha E_\alpha}{Rg(\alpha)}\right] - 5.331 - 1.052\frac{E_\alpha}{RT_{\alpha,i}} \tag{12}$$

KAS method

$$\ln\left(\frac{\beta_i}{T_{\alpha,i}^2}\right) = \ln\left[\frac{RA_\alpha}{E_\alpha g(\alpha)}\right] - \frac{E_\alpha}{RT_{\alpha,i}} \tag{13}$$

Starink method

$$\ln\left(\frac{\beta}{T^{1.92}}\right) = \ln\left[\frac{AR}{E_\alpha g(\alpha)}\right] - 1.0008\frac{E_\alpha}{RT_{\alpha,i}} \tag{14}$$

Four model-free methods are widely used to calculate kinetic parameters due to their simplicity and not requiring the selection of kinetic models. The four model-free methods used in this paper are all linear, and only the FR method can be used in the case of a nonlinear change of the heating rate. The activation energy results measured by FR and Starink methods may be more accurate. However, when using the FR method, the derivative is required to convert the data, which leads to numerical instability and noise sensitivity. The relative error of FWO and KAS methods is large. They are derived under the assumption that the activation energy is constant during the reaction process, and both use oversimplified temperature integral approximations.

2.3.3. Determination of Reaction Mechanism. To easily and quickly analyze the solid thermal decomposition reaction mechanism from DTG data, Criado developed a simple graphical method (Z-master plot), which can be described by eq.[28] The reaction mechanism was predicted by comparing the Z-master plot of the experimental values with the theoretical plot.[24]

https://doi.org/10.1021/acsomega.2c07379
ACS Omega 2023, 8, 13593−13604

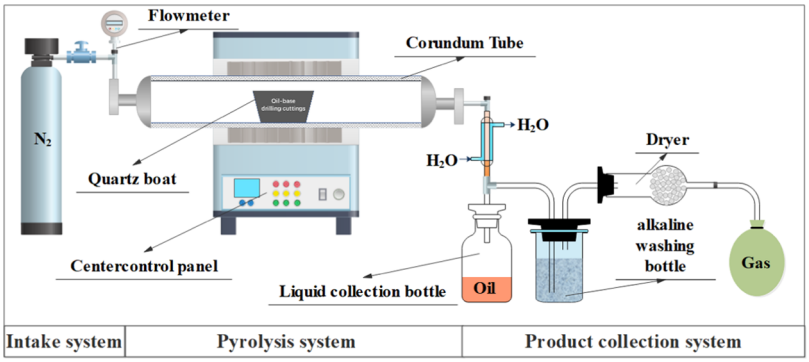

Figure 1. Experiment flowchart of tubular vacuum pyrolysis.

$$\frac{Z_\alpha}{Z_{0.5}} = \frac{f(\alpha)\cdot g(\alpha)}{f(0.5)\cdot g(0.5)} = \left(\frac{T_\alpha}{T_{0.5}}\right)^2 \cdot \left[\frac{(\mathrm{d}\alpha/\mathrm{d}T)_\alpha}{(\mathrm{d}\alpha/\mathrm{d}T)_{0.5}}\right] \quad (15)$$

From the left side of the equation above, equation $[f(\alpha)\cdot g(\alpha)/f(0.5)\cdot g(0.5)]$, combined with the various solid-state reaction mechanisms in Table 2, will give a Z-master plot of a theoretical curve. However, equation $\{(T_\alpha/T_{0.5})^2\cdot[(\mathrm{d}\alpha/\mathrm{d}t)_\alpha/(\mathrm{d}\alpha/\mathrm{d}t)_{0.5}]\}$ will obtain a Z-master plot of experimental values.[17] If taken as a reference value, then all Z-master graphs will intersect at $[Z_\alpha/Z_{0.5} = 1]$. By comparing the theoretical and experimental curves, the most suitable theoretical curve was selected as the reaction mechanism.[29,30]

The Z-main plot method can provide a suitable model for multiphase reactions, allowing rapid selection of a single mechanism or a group of mechanisms, reducing the workload of kinetic analysis. However, the calculation process needs to use a derivative to convert data, which may lead to theoretical errors.

2.4. Pyrolysis Experiments. *2.4.1. Pyrolysis Process.* The flowchart of the OBDC pyrolysis experiment is shown in Figure 1, which is mainly composed of a heating device (vacuum tube heating furnace), a distillate gas condensation device, and a product collection device. The chloroform-cleaned porcelain ark and the tubular heating furnace were prepared before the experiment. The OBDC samples were mixed evenly and filtered with a 1000-mesh sieve. The solid samples (laying thickness h_i) were taken and placed in a porcelain ark and pushed into a tubular heating furnace. The vacuum pump was turned on to draw out the air, purged with nitrogen to ensure the nitrogen atmosphere in the furnace, and the inlet and outlet valves were closed. A fixed heating rate T_i was set, and when the temperature rose to the target temperature T_g, it was kept at the target temperature for pyrolysis t_i time.

The experimental factors include the target temperature T_g (250, 300, 350, 400, 450, 500 °C), the residence time t_i (20, 35, 50, 65, 95 min), the heating rate T_i (10, 15, 20, 25, 30 °C/min), and the laying thickness h_i (4, 8, 12, 16, 20 mm). Among them, the treatment temperature and treatment time are the key factors in the pyrolysis process.[31,32] In order to reduce the number of experiments, the control variable method was used to design the experiment, and the four experimental factors were analyzed in turn. In the experiment, the gas phase flowing out of the gas outlet is liquefied by the condensing device and then enters the liquid phase collection bottle, and the tail gas enters the alkali washing collection bottle. The condensed liquid phase and the noncondensable gas are collected and detected, the weights of liquid phase and solid phase products are recorded, and the output of the gas and liquid is measured. The calculation formula of the recovery rate m_o of mineral oil (pyrolysis oil) is as follows

$$m_o = \frac{m_{oc} - m_{rc}}{m_{oc}} \times 100\% \quad (16)$$

where m_{oc} is the total oil content of OBDC samples, g; and m_{rc} is the oil content of residues after pyrolysis of OBDC samples, g

2.4.2. Product Analysis and Characterization. The composition of the mineral oil after pyrolysis was analyzed by gas chromatography-mass spectrometry (Agilent 7890B-5977A, GC-MS). Gas chromatography conditions: the chromatographic column (DB-5MS) is 60 m × 0.25 mm × 0.25 μm, constant flow mode, carrier gas is helium (purity not less than 99.999%), and the flow rate is 1.0 mL/min. The initial temperature of the heating program was 60 °C, held for 2 min, and raised to 280 °C at 10 °C/min, and held for 10 min; the injection port temperature was 270 °C; split injection with a split ratio of 2:1; the injection volume was 1 μL; a single quadrupole mass spectrometer detector, electron impact ion source (EI), the ion source temperature was 230 °C, the quadrupole temperature was 150 °C, the GC-MS interface temperature was 280 °C, and the solvent delay was 8 min. US EPA 8260C was used to determine C_6−C_9, and US EPA 8015C standards were used to determine C_{10}−C_{14}, C_{15}−C_{28}, and C_{29}−C_{36}.

The performance of recovered mineral oil was measured using a high-temperature roller heating furnace (XGRL-4A). The sample was stirred with a high-speed stirrer for 1 min, and it was poured into the liquid cup of the rotational viscometer to the mark so that the liquid level of the sample was flush with the upper end of the outer cylinder. The power switch of the rotational viscometer was turned on and rotated at 600 rpm; after the dial reached a stable reading value, the reading was recorded. In the same way, the stable value of the dial was recorded at 300 rpm. The values of PV, YP, and AV are calculated by the following formulas

$$\mathrm{PV} = \theta_{600} - \theta_{300} \quad (17)$$

$$\mathrm{YP} = 2\cdot\theta_{300} - \theta_{600} \quad (18)$$

$$\mathrm{AV} = \frac{1}{2}\theta_{600} \quad (19)$$

wherein PV is the plastic viscosity, mPa·s; YP is the dynamic shear force, Pa; AV is the apparent viscosity, mPa·s; θ_{600} is the

https://doi.org/10.1021/acsomega.2c07379
ACS Omega 2023, 8, 13593−13604

reading value of the 600 rpm dial; and θ_{300} is the reading value of the 300 rpm dial.

3. RESULTS AND DISCUSSION

3.1. TGA Analysis. The thermogravimetric (TGA) analysis results of OBDCs at different heating rates are shown in Figure 2. A low heating rate is helpful to study the pyrolysis of

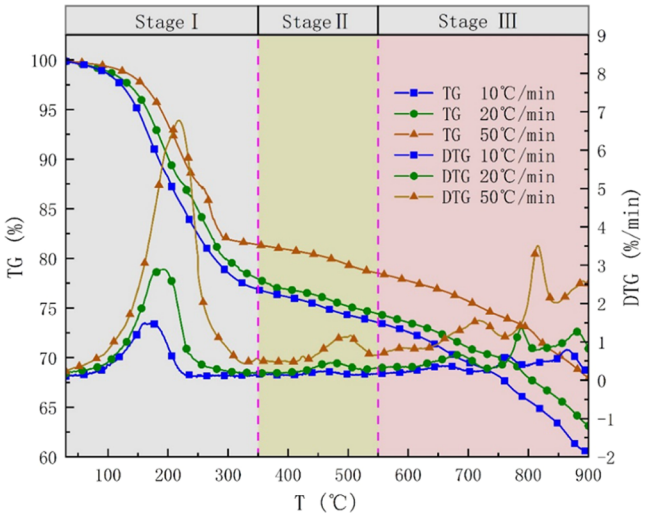

Figure 2. Thermogravimetric curves for heating rates of 10, 20, and 50 °C/min.

OBDCs, and a high heating rate is convenient to predict the pyrolysis mechanism. With the increase of the heating rate, the change trends of TG and DTG curves were basically consistent. According to the change trend of the TG/DTG curve, the thermal weight loss of OBDCs can be divided into three stages. The first stage is the rapid weight loss stage (below 350 °C), and the weight loss is about 18.6−23.1%. It is mainly the evaporation of water and light hydrocarbons, with less obvious fluctuations at 10 and 50 °C/min. It may be caused by the difference in the content of water and oil.[9] The second stage is the slow weight loss stage (350−550 °C), and the weight loss is about 2.9−3.5%. The main reason for the slow weight loss is the slow volatilization of heavy components and the decomposition of some macromolecular organics. Kinetic analysis and pyrolysis experiments are also performed at this stage. he third stage is a slower weight loss stage (550−900 °C), where the weight loss is about 10.6−12.9%. This stage is mainly due to the cracking and carbonization of complex hydrocarbons and the decomposition of inorganic minerals. Thermogravimetric results showed that the final residue was 60.5−67.9%, which was lower than the approximate analysis results in Table 1. The possible reason is that the thermogravimetric experiment selects a higher final pyrolysis temperature and residence time to make pyrolysis more sufficient, so the ash content is lower. The weight loss trend of OBDC is roughly the same under different heating rates, and the maximum weight loss rate increases with the increase of the heating rate. As the heating rate increases, the TG and DTG curves shift to the high-temperature region, and a similar phenomenon was also observed by Ni et al.[33] In addition, the peak of the TG curve in the third stage is because the increase of the heating rate will cause the secondary cracking reaction, the decomposition of inorganic substances, and the occurrence of coking.

3.2. Kinetic Analysis. *3.2.1. Activation Energy Assessment.* In the second stage of the subdivision of the OBDC pyrolysis process, the conversion ratios ranged from 0.1 to 0.9, and four isoconversion methods (FR, FWO, KAS, and Starink methods) were used to estimate the activation energy (E_α); the result is shown in Figure 3. E_α was calculated by the slope of the fitted curve; the calculation results are shown in Table 3, and the value of R^2 was between 0.96875 and 0.9995. The average activation energies obtained by FR, FWO, KAS, and Starink methods were 185.5, 184.16, 166.17, and 176.03 kJ/mol, respectively. The average activation energy is larger compared to the results of OBDC pyrolysis by Lv et al.[13] This may be because the OBDCs require less energy to volatilize the light components in the low-temperature pyrolysis stage (80−360 °C). In the middle- and low-temperature stages (350−550 °C), the pyrolysis reaction of heavy components is more difficult and requires more energy. This means that more energy is required to thoroughly dispose of the oil in the OBDCs.

The KAS and Starink methods obtained relatively low values of 166.17 and 176.03 kJ/mol, respectively, probably due to different approximations and assumptions during the derivation of the different models.[34] The average activation energies estimated by FR and FWO methods are very close, which are 185.5 and 184.16 kJ/mol, respectively. It may be more suitable than KAS and Starink methods to estimate the activation energy of OBDCs. In addition, it can be seen that the activation energy increases dynamically with the increase of conversion rate.

3.2.2. Prediction of Reaction Mechanism. The mineral oil component in OBM is a mixture containing hydrocarbons such as alkanes, aromatic hydrocarbons, and additives. After drilling, due to the influence of the high-temperature environment and the introduction of impurities, the composition of waste OBDC becomes more complicated. Therefore, it is very difficult to accurately describe the pyrolysis process of waste OBDCs. Based on the Z-master diagram of Criado,[35] this study predicts the mechanism during the pyrolysis of OBDCs. Figure 4a shows the relationship between the experimental curve and the conversion at different heating rates. It can be seen that the experimental curve changes continuously with the conversion rate, and each conversion rate follows a different kinetic model.

Figure 4b is the Z-master diagram at 10 °C/min; the conversion rate of 0.1−0.2 changed from the R3 model to the R6 model, 0.2−0.4 changed from the R6 model to the P4 model, 0.4−0.7 followed the F1 model, 0.7−0.8 changed from the F1 to F3 model, and 0.8−0.9 followed the F3 model. Figure 4c is the Z-master diagram at 20 °C/min; the conversion rate of 0.1−0.3 changed from the R6 model to the F1 model, 0.3−0.6 followed the F1 model, 0.6−0.7 followed the D2 model, 0.7−0.8 changed from the D2 model to the F3 model, and 0.8−0.9 followed the F3 model. Figure 4d is the Z-master diagram at 50 °C/min; the conversion rate of 0.1−0.2 changed from the R6 model to the R1 model, 0.2−0.5 followed the R1 model, 0.5−0.6 followed the P4 model, 0.6−0.7 followed the D2 model, 0.7−0.8 changed from the D2 model to the F3 model, and 0.8−0.9 followed the F3 model. Table 4 shows the transformation process of the OBDC pyrolysis model at different heating rates. It can be seen that the reaction mechanism of OBDC is very complex at lower heating rates, which may be the reason why higher heating rates were chosen to predict the solid reaction mechanism.[16]

https://doi.org/10.1021/acsomega.2c07379
ACS Omega 2023, 8, 13593−13604

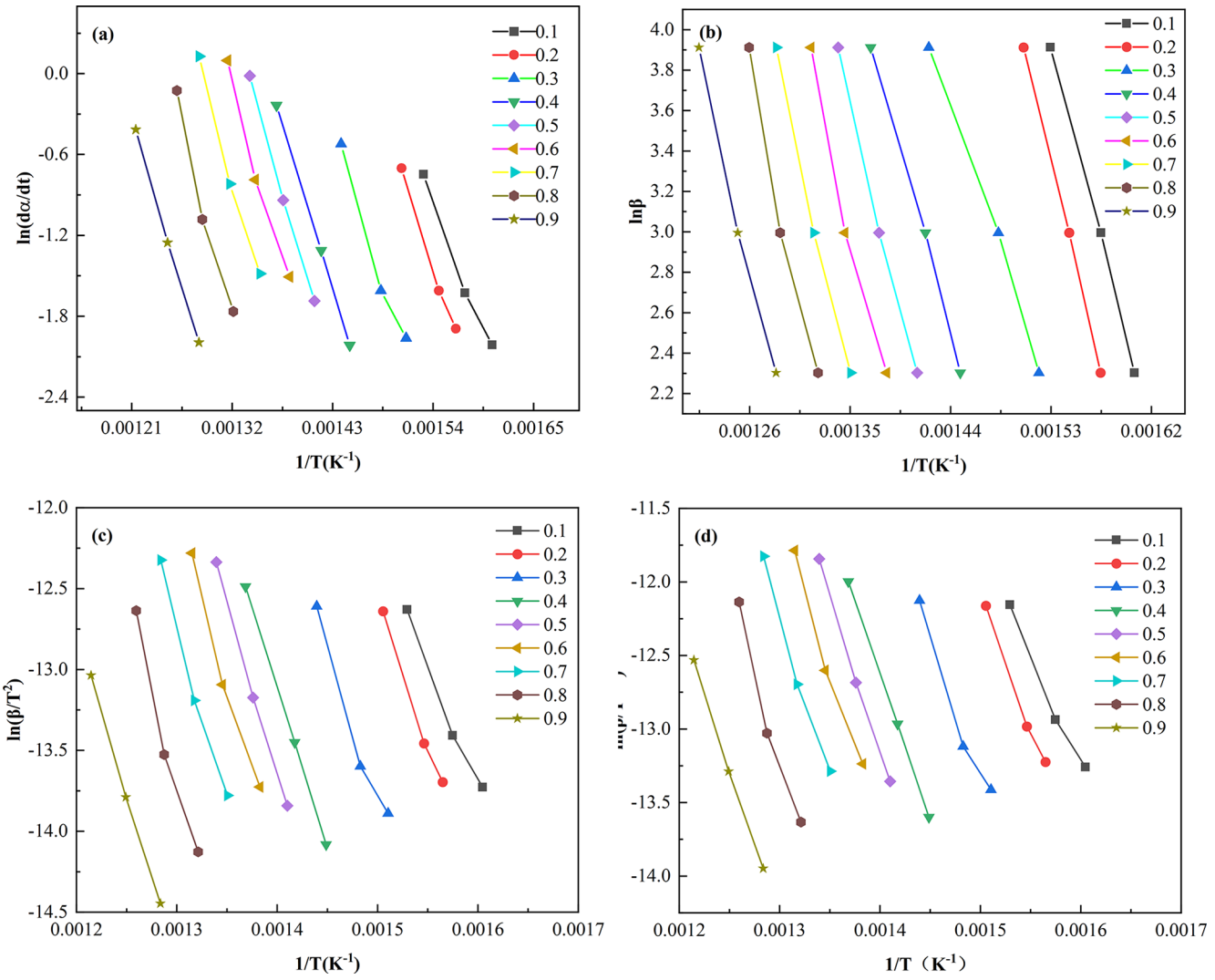

Figure 3. Iso-conversional models for kinetic analyses of OBDCs: (a) FR, (b) FWO, (c) KAS, and (d) Starink methods.

Table 3. OBDC Pyrolysis Activation Energies Obtained Using Different Model-Free Methods

	FR		FWO		KAS		Starink	
conversion	E_α (kJ/mol)	R^2	E_α (kJ/mol)	R^2	E_α (kJ/mol)	R^2	E_α (kJ/mol)	R^2
0.1	141.54	0.98916	168.34	0.99858	122.99	0.98574	123.63	0.98591
0.2	169.39	0.99311	207.89	0.98245	150.74	0.99134	151.36	0.99142
0.3	171.93	0.97501	177.61	0.99779	153.04	0.96875	153.67	0.96905
0.4	184.19	0.99995	157.51	0.99770	164.99	0.99994	165.63	0.99994
0.5	196.55	0.99837	180.05	0.99644	177.18	0.99802	260.88	0.99803
0.6	195.51	0.98581	186.19	0.98055	175.99	0.98264	176.63	0.98278
0.7	201.66	0.99038	191.31	0.99402	181.93	0.98828	182.58	0.98838
0.8	218.67	0.97650	204.32	0.98128	198.766	0.9718	199.4	0.97201
0.9	190.07	0.99891	184.25	0.99413	169.86	0.99868	170.53	0.99869
average	185.50		184.16		166.17		176.03	

3.3. Pyrolysis Experiment. *3.3.1. Pyrolysis Process.* Figure 5 shows the variation law of oil content and the mineral oil recovery rate of OBDC residues under the same conditions as six target temperatures and residence times. With increasing target temperature and residence time, the oil content of OBDCs decreased from 8.03% (250 °C, 20 min) ~1.87% (250 °C, 95 min) to 0.89% (500 °C, 20 min) ~0.25% (500 °C, 95 min). When the target temperature was lower than 350 °C, the oil content of the OBDC residue decreased significantly, and the oil content declined gradually after 350 °C, which is consistent with the results of the thermogravimetric experiment. In addition, with the continuous volatilization of the liquid phase of OBDC, the thermal conductivity of the oil-containing solid phase also decreased,[36,37] which caused the oil content of the residue to stabilize.

As shown in Figure 5c, at 250−350 °C, the oil content of the OBDC residue decreased from 2.58 to 0.50%, which was the fastest decline, and the mineral oil recovery rate was 85.92−

https://doi.org/10.1021/acsomega.2c07379
ACS Omega 2023, 8, 13593−13604

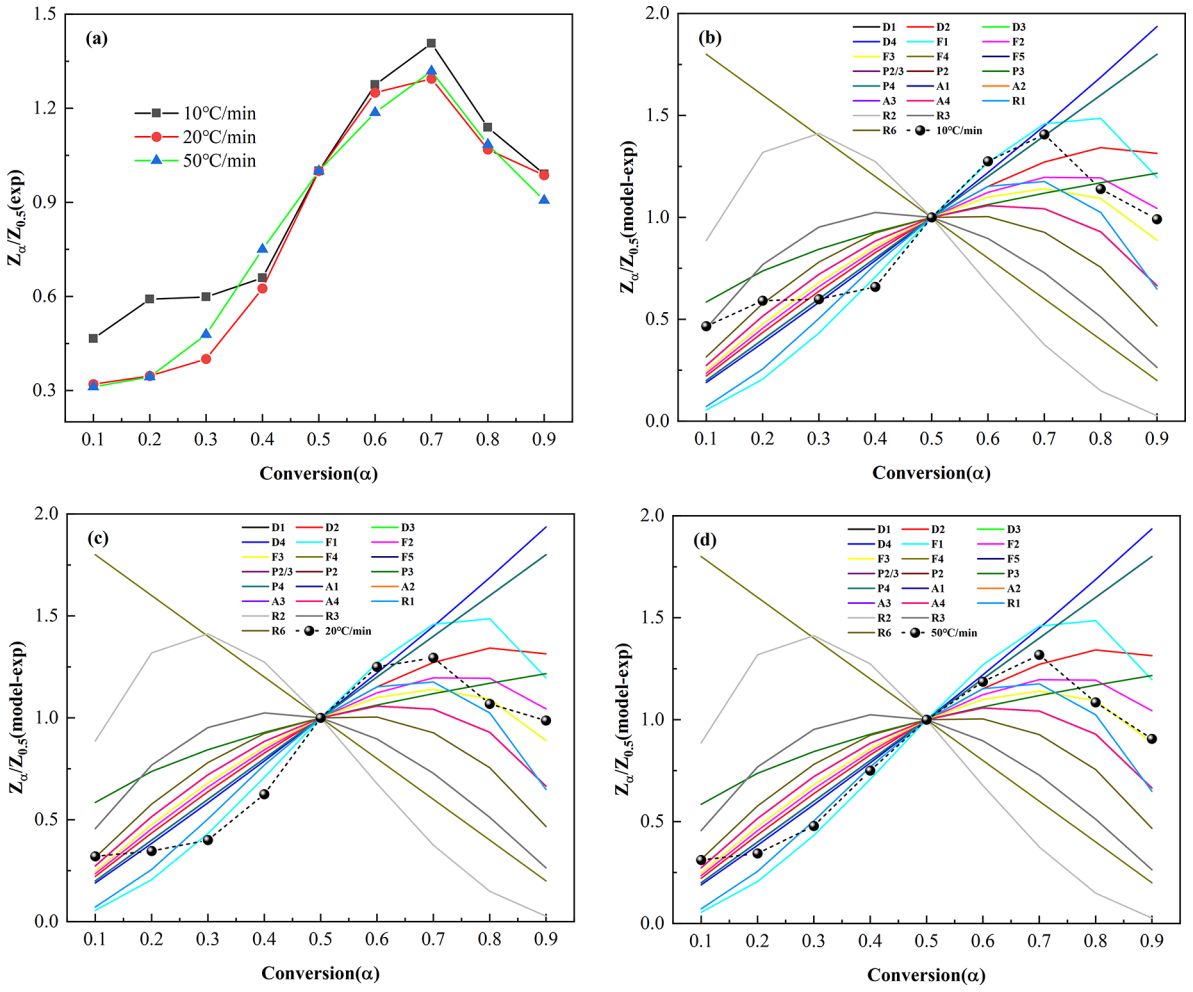

Figure 4. Experimental and theoretical Z-master plots for predicting reaction mechanisms: (a) Z-master plot of experiments at different heating rates; (b) Z-master plot at 10 °C/min; (c) Z-master plot at 20 °C/min; and (d) Z-master plot at 50 °C/min.

Table 4. Pyrolysis Model Transition at Different Heating Rates

	heating rate (°C/min)		
conversion	10	20	50
0.1−0.2	R3-R6	R6-F1	R6-R1
0.2−0.3	R6-P4	R6-F1	R1
0.3−0.4	R6-P4	F1	R1
0.4−0.5	F1	F1	R1
0.5−0.6	F1	F1	P4
0.6−0.7	F1	D2	D2
0.7−0.8	F1-F3	D2-F3	D2-F3
0.8−0.9	F3	F3	F3

98.38%. When the residence time is more than 50 min and the target temperature exceeds 350 °C, the residual oil content is less than 0.3 % (as shown in the powder column), which meets the "Agricultural Sludge Pollutant Control Standard",[38] and the recovery rate of mineral oil is higher than 98.43 %. As shown in Figure 6, when the residence time is within 50 min, changing the target temperature has a greater impact on the change of the residual oil content, and when the residence time exceeds 50 min, changing the temperature has a smaller effect on the change of the residual oil content. In the range of 50 min, the final temperature of pyrolysis is prolonged. On the one hand, light compounds are heated for a longer time and volatilized more fully. On the other hand, it also makes the reaction of the organic matter reacting at this temperature more complete. Therefore, the corresponding oil content gradually decreased. When the final temperature of pyrolysis was 95 min (as shown in Figure 5f), the oil content decreased slowly. This is because with the progress of the pyrolysis reaction, the macromolecular organic matter in the OBDC is continuously decomposed, and the light components and small molecular substances are generated.

Through the above analysis, we take the target temperature of 350 °C and the residence time of 50 min, with the other conditions remaining the same, to study the effect of laying thickness (4, 8, 12, 16, 20 mm) on the solid phase oil content and yield of OBDC, and the results are shown in Figure 7. According to the residual oil content, the laying thickness of OBDC has a great influence on the pyrolysis effect. With the increase of laying thickness, the residual oil content gradually increases after pyrolysis, and the mineral oil recovery rate gradually decreases. The reason may be that the pyrolysis process is a physical reaction, and the mineral oil in the OBDC is separated from the solid cuttings by volatilization. Therefore, the thinner the laying thickness is, the more easily the light mineral oil molecules are volatilized by heat, while increasing the laying thickness will make it difficult for the mineral oil in the lower OBDC to diffuse. When the laying thickness is 20 mm, the oil content of the residue reaches 0.35%. In order to

https://doi.org/10.1021/acsomega.2c07379
ACS Omega 2023, 8, 13593−13604

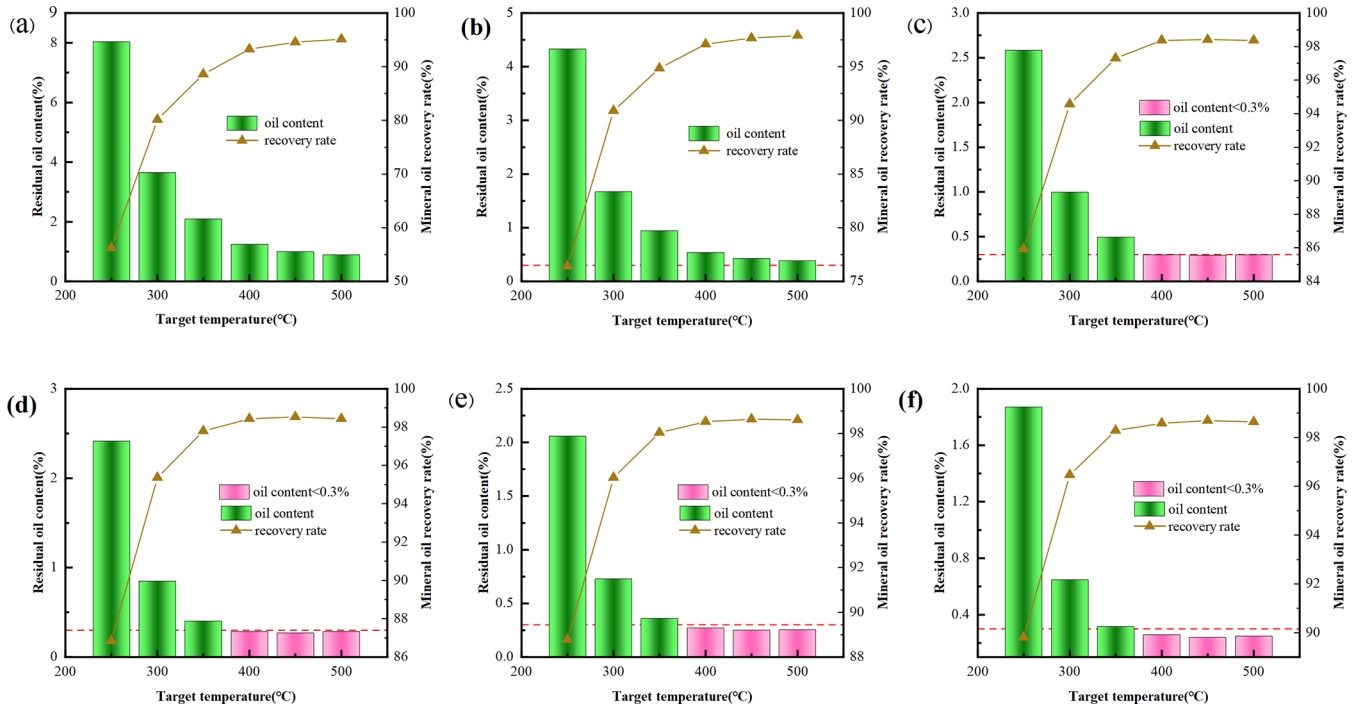

Figure 5. Oil content and mineral oil recovery of OBDC ash residue at different target temperatures and residence times: (a) 20 min, (b) 35 min, (c) 50 min, (d) 65 min, (e) 80 min, and (f) 95 min.

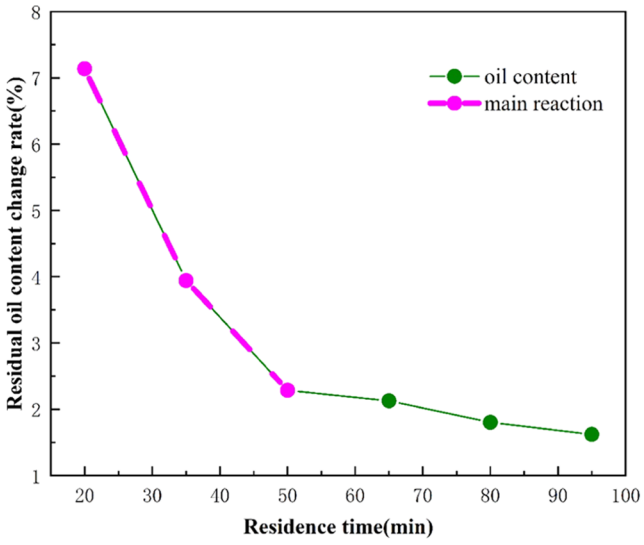

Figure 6. Relationship between residence time and rate of change of residual oil content.

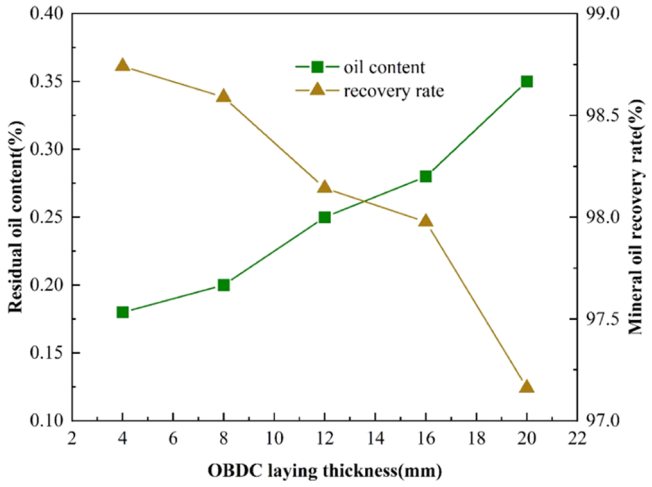

Figure 7. Effect of laying thickness on residual oil content and mineral oil yield.

meet the "Agricultural Sludge Pollutant Control Standard", the laying thickness should be controlled within 20 mm as much as possible.

The heating rates were 10, 15, 20, 25, and 30 °C/min for pyrolysis experiments. Other experimental conditions (350 °C, 50 min, 16 mm) were unchanged. The results are shown in Figure 8. During the process of gradually increasing the heating rate from 5 to 30 °C/min, the oil content of OBDC changed from 0.26 to 0.55%, and the change was the largest in the process of 25−30 °C/min. The weight loss rate was reduced from 14.18 to 13.2%. This may be because the OBDCs reach the target temperature more quickly as the heating rate increases, resulting in a shorter residence time. The corresponding reaction time of the substances reacted in the high-temperature section is shortened, and the pyrolysis is terminated before the reaction is completed, which reduces the degree of the reaction. At the same time, the high heating rate will also lead to uneven heating inside the OBDC. Before the external temperature can be transmitted to the interior, coke bodies form on the surface, which hinders the escape of oil substances, resulting in an incomplete reaction. Therefore, reducing the heating rate helps oil recovery.

In short, in order to improve the yield of mineral oil and make the oil content of the residue less than 0.3 %, experiments were designed for four key process parameters. Through the transition conditions of the experiment, the effects of different process parameters on the yield of mineral

https://doi.org/10.1021/acsomega.2c07379
ACS Omega 2023, 8, 13593−13604

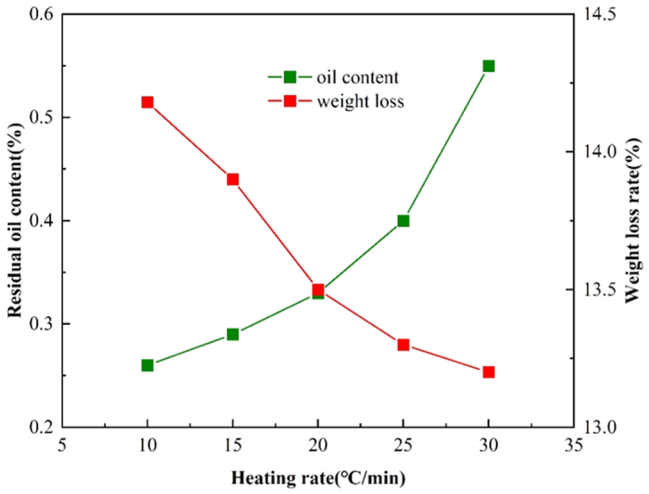

Figure 8. Oil content and weight loss of OBDCs under different heating rates.

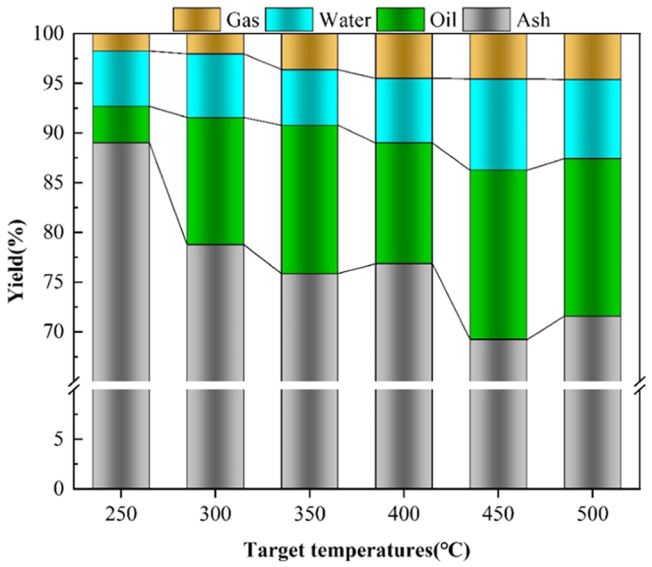

Figure 9. Product yield of the OBDC pyrolysis experiment.

oil and the residual oil content are obtained as shown in Table 5.

3.3.2. Experimental Product. In order to further study the target temperature and product evolution characteristics, the target temperatures were taken as 250, 300, 350, 400, 450, and 500 °C, the residence time was 50 min, the laying thickness was 16 mm, and the heating rate was 10 °C/min. The pyrolysis product distribution is shown in Figure 9.

As the pyrolysis temperature increases, the product yields of various states change significantly. Among them, the highest proportion of solid phase (more than 70%) is the main product. When the temperature is 350−400 °C, the solid phase yield remains basically unchanged. The main reason is that the oil phase and water phase of oil-based drilling cuttings are basically volatilized completely at 350−400 °C, and the remaining solid phase is mainly the minerals added in the formation and drilling process and a small amount of heavy components. When the temperature exceeds 400 °C, the minerals and organic matter in the oil-based drilling cuttings will interact. At higher temperatures, decarboxylation, deamination, and other reactions will occur to form low-molecular-weight alkanes, cycloalkanes, and aromatic hydrocarbons. The oil phase yield increased with the increase of temperature, reaching a maximum of 17.04% at 450 °C, and then decreased to 15.87% at 500 °C. The reason for this phenomenon is that when the temperature reaches 450 °C, the oil phase hydrocarbons are cracked to form small molecular compounds such as noncondensable gases, resulting in an increase in gas phase yield. The aqueous phase yield reaches a maximum of 9.16% at 450 °C, which is slightly higher than the water content of the oil-based drilling cutting sample. The possible reason is that high temperature is conducive to dehydration reaction and degradation of polymer compounds. At 500 °C, it dropped to 7.94%; the reason for this phenomenon is that when the temperature is higher than 450 °C, the aqueous phase is involved in the solid or liquid phase chemical reaction. When the gas phase yield reaches 400 °C, it is stable at about 4.4%, and then, with the increase of temperature, a secondary cracking reaction occurs to generate small molecular gaseous products, which increases the gas yield.[39,40]

3.3.3. Comparison of Mineral Oils before and after Pyrolysis. The 400 °C experimental group mineral oil in the product was taken and analyzed by GC-MS. The analysis results are shown in Figure 10.

The distribution of recovered mineral oil components before and after pyrolysis of OBDC is not much different, in which C_{15}−C_{28} decreased by 3.26% and C_{10}−C_{14} increased by 2.89%. This is because there is a cracking reaction in the heavy oil (C_{15}−C_{28}) during the pyrolysis process, and part of the light oil (C_{10}−C_{14}) escapes and volatilizes.[41] The heavy components (C_{29}−C_{36}) increased slightly, partly because of the volatilization of light oil and partly because the mineral oil was easily aged to form heavy components under high-temperature conditions.[42] The PAHs in the mineral oil before pyrolysis were mainly 2, 3, and 4 rings, and after pyrolysis, they tended to change to 4, 5, and 6 rings. During the pyrolysis process, the temperature is relatively high, the low-molecular-weight PAHs with small molecular weights are easily dissipated, and the percentage of medium- and high-cyclic PAHs increases; the

Table 5. Effects of Different Process Parameters on the Yield of Mineral Oil and the Oil Content of Residue

process variable	condition	yield of mineral oil (m_o)	residual oil content (m_{rc})
target temperature (T_g, °C)	<350	significantly higher (56.24−98.28%)	decreased significantly (0.32−8.03%); minimum up to 0.315%
	>350	the yield is stable (93.25−98.64%)	changed to be steady (0.25−1.24%); t_i > 50 min, m_{rc} < 0.3%
residence time (t_i, min)	<50	T_g has a great influence on m_o (56.24−98.38%)	T_g has a great influence on m_{rc} (0.30−8.03%)
	>50	the yield is stable (86.84−98.64%)	T_g has little effect on m_{rc}; T_g > 350 °C, m_{rc} < 0.3%
laying thickness (n_i, mm)	<16	97.98−98.74%	m_{rc} < 0.3%
	>16	97.16%	0.35%
heating ate (T_i, °C/min)	<20	helps improve m_o	m_{rc} < 0.3%
	>20	the weight loss rate changed greatly	m_{rc} > 0.3% (0.33−0.55%)

https://doi.org/10.1021/acsomega.2c07379
ACS Omega 2023, 8, 13593−13604

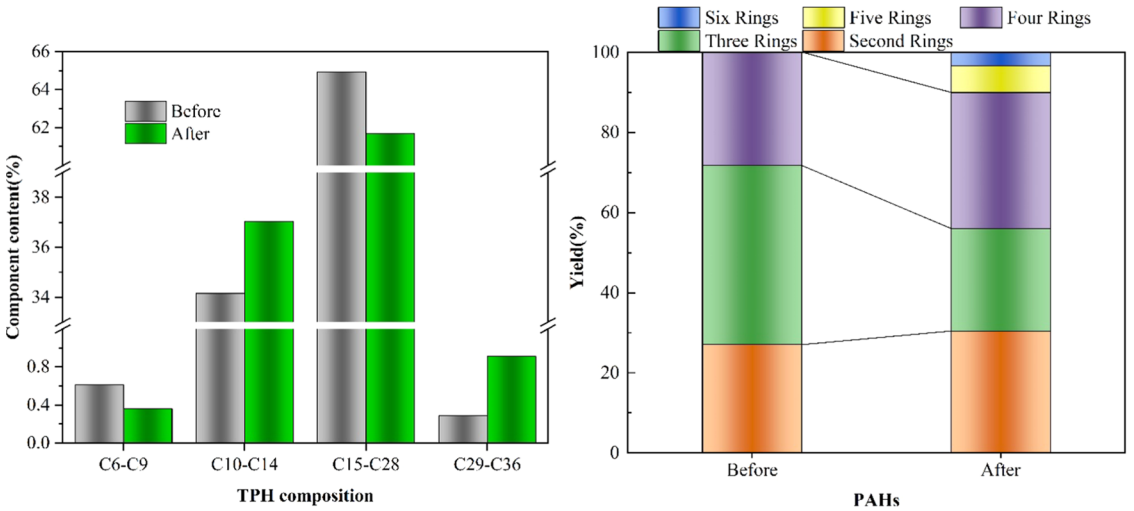

Figure 10. Contents of TPH and PAH in mineral oil before and after pyrolysis.

distribution of PAHs largely depends on the pyrolysis temperature.[43]

3.4. Evaluation of the Performance of Recovered Mineral Oil. The OBM was prepared with 0# diesel oil and recycled mineral oil as the base oil, and the performance of the OBM was evaluated by using a hot rolling furnace (XGRL-4A high-temperature rolling furnace). The results are shown in Table 6.

Table 6. Performance Comparison of OBM Prepared from Recovered Mineral Oil and 0# Diesel[a]

base oil	state	PV (mPa·s)	YP (Pa)	YP/PV (Pa/mPa·s)	Φ6/Φ3	ES (V)
0# diesel	before	40.7	13.5	0.3317	3/2	642
	after	45.5	17.5	0.3846	7/6	750
recovered mineral oil	before	43.5	14.2	0.3264	4/3	685
	after	45.6	17.3	0.3794	7/6	775

[a]Note: the test conditions are 120 °C hot rolling for 16 h, 50 °C test rheology, high-temperature and high-pressure water loss test conditions are 70 °C × 30 min × 500 psi.

It can be seen from Table 6 that the performance of the OBDC fluid prepared from refined oil and recovered mineral oil is not much different after rolling and has good rheology and emulsion stability. The milk voltage is greater than 600 V. Among them, the demulsification voltage of the drilling fluid prepared for the recovered mineral oil is slightly increased, mainly because the recovered mineral oil is more complex than the diesel oil. Among them, the colloid has many condensed aromatic ring structures (number of aromatic rings, aromatic lamellae) and alkyl side-chain structures, with strong polarity and good dispersion stability of the system. In addition, the content of branched alkanes in the recovered mineral oil is also higher than that in diesel oil, and it contains more polar hydrocarbons and other impurities, which increases the stability of the mineral oil and causes a slight increase in the demulsification voltage.

4. CONCLUSIONS

The OBDCs were pyrolyzed at heating rates of 10, 20, and 50 °C/min by a TGA analyzer. The pyrolysis of OBDCs is divided into three stages, and the main reaction of OBDC occurs in the second stage (350−550 °C). The average activation energies obtained by FR, FWO, KAS, and Starink methods are 185.5, 184.16, 166.17, and 176.03 kJ/mol, respectively. The average activation energy estimated by FR and FWO methods is very close. In addition, as the pyrolysis process progresses, the required activation energy also increases. Under different conversion rates and heating rates, the kinetic models followed are different, which also shows that the mechanism of OBDC pyrolysis process is very complex, and it is difficult to describe the whole reaction process with one or several reactions.

In addition, the effect of process parameters of OBDC pyrolysis on product yield was studied by a vacuum tube furnace. The results showed that when the target temperature was higher than 350 °C and the residence time was higher than 50 min, the residual oil content was lower than 0.3% of the "agricultural sludge pollutant control standard", and the mineral oil recovery rate was higher than 98.43%. Laying thickness less than 20 mm can guarantee the oil content index. Heating rate below 15 °C/min helps oil recovery. The main product after pyrolysis is the solid phase, accounting for more than 70%. Interestingly, when the temperature increases from 450 to 500 °C, the oil phase yield decreases instead. The petroleum hydrocarbons and aromatic hydrocarbons in mineral oil before and after pyrolysis did not change much. In addition, OBMs were prepared with recycled mineral oil and 0# diesel oil, respectively, for hot rolling experiments, and the rheological properties and emulsifying properties were analyzed and compared. The results show that the demulsification voltage of the drilling fluid with recovered mineral oil increases slightly, and the performance before and after hot rolling is comparable. It can be directly used to configure OBM, reduce production costs, and realize resource recycling.

In summary, analyzing the kinetics and reaction mechanism of OBDC pyrolysis is helpful to optimize the process parameters and improve the yield of recovered mineral oil. It provides data support for the study of a new OBDC pyrolysis reactor. This study can improve the resource utilization effect of OBDC pyrolysis, which is of great significance to the green development of shale gas.

https://doi.org/10.1021/acsomega.2c07379
ACS Omega 2023, 8, 13593−13604

AUTHOR INFORMATION

Corresponding Author

Quanlin Xiao − *School of Mechanical Engineering, Sichuan University of Science & Engineering, Yibin 644000 Sichuan, China;* orcid.org/0000-0002-3902-729X; Email: xiaoquanlin.com@qq.com

Authors

Pu Liu − *School of Mechanical Engineering, Sichuan University of Science & Engineering, Yibin 644000 Sichuan, China; Over-control Lab, Sichuan University of Science & Technology, Yibin 644000 Sichuan, China*

Ning Dai − *PetroChina Offshore Emergency Rescue Response Center, Tangshan 063000 Hebei, China*

Zhongbin Liu − *School of Mechanical Engineering, Sichuan University of Science & Engineering, Yibin 644000 Sichuan, China; Over-control Lab, Sichuan University of Science & Technology, Yibin 644000 Sichuan, China*

Chenlong Wang − *CNPC Engineering Technology R&D Company Limited, Tianjin 300451, China*

Complete contact information is available at: https://pubs.acs.org/10.1021/acsomega.2c07379

Notes

The authors declare no competing financial interest.

ACKNOWLEDGMENTS

This work was supported by The Project of Sichuan University of Science & Engineering (No. 2020RC18) and The Key Project of Sichuan Provincial Key Lab of Process Equipment and Control (No. GK202007). The authors gratefully acknowledge the financial support received.

REFERENCES

(1) Zou, C.; Zhao, Q.; Cong, L.; Wang, H.; Shi, Z.; Wu, J.; Pan, S. Development progress, potential and prospects of shale gas in China. *J. Tianranqi Gongye* **2021**, *41*, 1−14.

(2) Yang, H.; Diao, H.; Zhang, Y.; Xia, S. Treatment and novel resource-utilization methods for shale gas oil based drill cuttings - a review. *J. Environ. Manage.* **2022**, *317*, No. 115462.

(3) Daae, H. L.; Heldal, K. K.; Madsen, A. M.; Olsen, R.; Skaugset, N. P.; Graff, P. Occupational exposure during treatment of offshore drilling waste and characterization of microbiological diversity. *Sci. Total Environ.* **2019**, *681*, 533−540.

(4) Hu, G.; Liu, H.; Chen, C.; Hou, H.; Li, J.; Hewage, K.; Sadiq, R. Low-temperature thermal desorption and secure landfill for oil-based drill cuttings management: pollution control, human health risk, and probabilistic cost assessment. *J. Hazard. Mater.* **2021**, *410*, No. 124570.

(5) Adhami, S.; Jamshidi-Zanjani, A.; Darban, A. K. Remediation of oil-based drilling waste using the electrokinetic-fenton method. *Process Saf. Environ. Protect.* **2021**, *149*, 432−441.

(6) Lv, Q.; Wang, L. A.; Jiang, J.; Ma, S.; Liu, L.; Zhou, Z.; Liu, L.; Wang, X.; Bai, J. Catalytic pyrolysis of oil-based drill cuttings over metal oxides: the product properties and environmental risk assessment of heavy metals in char. *Process Saf. Environ. Protect.* **2022**, *159*, 354−361.

(7) National Hazardous Waste List (2021 Edition) *J. Gazette State Council P. R. China*, **2008** No.128534 18−41.

(8) Feng, Y.; Tao, Y.; Meng, Q.; Qu, J.; Ma, S.; Han, S.; Zhang, Y. Microwave-combined advanced oxidation for organic pollutants in the environmental remediation: an overview of influence, mechanism, and prospective. *Chem. Eng. J.* **2022**, *441*, No. 135924.

(9) Chen, Z.; Zhou, J.; Chen, Z.; Chen, H.; Chen, Q.; He, C.; Liu, X.; Yuanjian, X. A laboratory evaluation of superheated steam extraction process for decontamination of oil-based drill cuttings. *J. Environ. Chem. Eng.* **2018**, *6*, 6691−6699.

(10) Xia, Z.; Yang, H.; Sun, J.; Zhou, Z.; Wang, J.; Zhang, Y. Co-pyrolysis of waste polyvinyl chloride and oil-based drilling cuttings: pyrolysis process and product characteristics analysis. *J. Cleaner Prod.* **2021**, *318*, No. 128521.

(11) Hu, G.; Liu, H.; Rana, A.; Li, J.; Bikass, S.; Hewage, K.; Sadiq, R. Life cycle assessment of low-temperature thermal desorption-based technologies for drill cuttings treatment. *J. Hazard. Mater.* **2021**, *401*, No. 123865.

(12) Choudhury, N. D.; Bhuyan, N.; Bordoloi, N.; Saikia, N.; Kataki, R. Production of bio-oil from coir pith via pyrolysis: kinetics, thermodynamics, and optimization using response surface methodology. *Biomass Convers. Biorefin.* **2020**, *11*, 2881−2898.

(13) Lv, Q.; Wang, L.; Ma, S.; Jiang, J.; Liu, L.; Zhou, Z.; Liu, L.; Wang, X.; Bai, J. Pyrolysis of oil-based drill cuttings from shale gas field: kinetic, thermodynamic, and product properties. *Fuel* **2022**, *323*, No. 124332.

(14) Qu, Y.; Li, A.; Wang, D.; Zhang, L.; Ji, G. Kinetic study of the effect of in-situ mineral solids on pyrolysis process of oil sludge. *Chem. Eng. J.* **2019**, *374*, 338−346.

(15) Liu, H.; Xu, G.; Li, G. Pyrolysis characteristic and kinetic analysis of sewage sludge using model-free and master plots methods. *Process Saf. Environ. Protect.* **2021**, *149*, 48−55.

(16) Singh, B.; Singh, S.; Kumar, P. In-depth analyses of kinetics, thermodynamics and solid reaction mechanism for pyrolysis of hazardous petroleum sludge based on isoconversional models for its energy potential. *Process Saf. Environ. Protect.* **2021**, *146*, 85−94.

(17) Singh, S.; Chakraborty, J. P.; Mondal, M. K. Intrinsic kinetics, thermodynamic parameters and reaction mechanism of non-isothermal degradation of torrefied acacia nilotica using isoconversional methods. *Fuel* **2020**, *259*, No. 116263.

(18) Ali, I.; Bahaitham, H.; Naebulharam, R. A comprehensive kinetics study of coconut shell waste pyrolysis. *Bioresour. Technol.* **2017**, *235*, 1−11.

(19) Yin, H.; Huang, X.; Song, X.; Miao, H.; Mu, L. Co-pyrolysis of de-alkalized lignin and coconut shell via tg/dtg-ftir and machine learning methods: pyrolysis characteristics, gas products, and thermokinetics. *Fuel* **2022**, *329*, No. 125517.

(20) Alsaedi, A. A.; Hossain, M. S.; Balakrishnan, V.; Abdul Hakim Shaah, M.; Mohd Zaini Makhtar, M.; Ismail, N.; Naushad, M.; Bathula, C. Extraction and separation of lipids from municipal sewage sludge for biodiesel production: kinetics and thermodynamics modeling. *Fuel* **2022**, *325*, No. 124946.

(21) Raza, M.; Inayat, A.; Ahmed, A.; Jamil, F.; Ghenai, C.; Naqvi, S. R.; Shanableh, A.; Ayoub, M.; Waris, A.; Park, Y. Progress of the pyrolyzer reactors and advanced technologies for biomass pyrolysis processing. *Sustainability* **2021**, *13*, 11061.

(22) GB/T 15555.12-1995, Determination of corrosivity of solid waste by glass electrode method *National Standard of China* .

(23) GB/T 212-2008, Industrial Analysis Methods for Coal *National Standard of China*.

(24) Dhyani, V.; Kumar, J.; Bhaskar, T. Thermal decomposition kinetics of sorghum straw via thermogravimetric analysis. *Bioresour. Technol.* **2017**, *245*, 1122−1129.

(25) Cai, J.; Xu, D.; Dong, Z.; Yu, X.; Yang, Y.; Banks, S. W.; Bridgwater, A. V. Processing thermogravimetric analysis data for isoconversional kinetic analysis of lignocellulosic biomass pyrolysis: case study of corn stalk. *Renewable Sustainable Energy Rev.* **2018**, *82*, 2705−2715.

(26) Mong, G. R.; Chong, W. W. F.; Nor, S. A. M.; Ng, J.; Chong, C. T.; Idris, R.; Too, J.; Chiong, M. C.; Abas, M. A. Pyrolysis of waste activated sludge from food manufacturing industry: thermal degradation, kinetics and thermodynamics analysis. *Energy* **2021**, *235*, No. 121264.

(27) Liu, H.; Wang, C.; Zhang, J.; Zhao, W.; Fan, M. Pyrolysis kinetics and thermodynamics of typical plastic waste. *Energy Fuels* **2020**, *34*, 2385−2390.

(28) Criado, J. M. Kinetic analysis of dtg data from master curves. *Thermochim. Acta* **1978**, *24*, 186−189.
(29) Alam, M.; Bhavanam, A.; Jana, A.; Viroja, J. K. S.; Peela, N. R. Co-pyrolysis of bamboo sawdust and plastic: synergistic effects and kinetics. *Renewable Energy* **2020**, *149*, 1133−1145.
(30) Doddapaneni, T. R. K. C.; Konttinen, J.; Hukka, T. I.; Moilanen, A. Influence of torrefaction pretreatment on the pyrolysis of eucalyptus clone: a study on kinetics, reaction mechanism and heat flow. *Ind. Crops Prod.* **2016**, *92*, 244−254.
(31) Falciglia, P. P.; Giustra, M. G.; Vagliasindi, F. G. A. Low-temperature thermal desorption of diesel polluted soil: influence of temperature and soil texture on contaminant removal kinetics. *J. Hazard. Mater.* **2011**, *185*, 392−400.
(32) Sang, Y.; Yu, W.; He, L.; Wang, Z.; Ma, F.; Jiao, W.; Gu, Q. Sustainable remediation of lube oil-contaminated soil by low temperature indirect thermal desorption: removal behaviors of contaminants, physicochemical properties change and microbial community recolonization in soils. *Environ. Pollut.* **2021**, *287*, No. 117599.
(33) Ni, Z.; Bi, H.; Jiang, C.; Sun, H.; Zhou, W.; Qiu, Z.; He, L.; Lin, Q. Influence of biomass on coal slime combustion characteristics based on tg-ftir, principal component analysis, and artificial neural network. *Sci. Total Environ.* **2022**, *843*, No. 156983.
(34) Kaur, R.; Gera, P.; Jha, M. K.; Bhaskar, T. Pyrolysis kinetics and thermodynamic parameters of castor (ricinus communis) residue using thermogravimetric analysis. *Bioresour. Technol.* **2018**, *250*, 422−428.
(35) Criado, J. M. Kinetic Analysis of DTG Data from Master Curves *Thermochimica Acta* 1978.
(36) Abu-Hamdeh, N. H.; Khdair, A. I.; Reeder, R. C. A comparison of two methods used to evaluate thermal conductivity for some soils. *Int. J. Heat Mass Transfer* **2001**, *44*, 1073−1078.
(37) Zhao, T.; Liu, S.; Xu, J.; He, H.; Wang, D.; Horton, R.; Liu, G. Comparative analysis of seven machine learning algorithms and five empirical models to estimate soil thermal conductivity. *Agric. For. Meteorol.* **2022**, *323*, No. 109080.
(38) GB / T 212-2008, Agricultural Sludge Pollutant Control Standard *National Standard of China*.
(39) Li, J.; Zheng, F.; Li, Q.; Farooq, M. Z.; Lin, F.; Yuan, D.; Yan, B.; Song, Y.; Chen, G. Effects of inherent minerals on oily sludge pyrolysis: kinetics, products, and secondary pollutants. *Chem. Eng. J.* **2022**, *431*, No. 133218.
(40) Liuyang, X.; Yang, H.; Huang, S.; Zhang, Y.; Xia, S. Resource utilization of secondary pyrolysis oil-based drilling cuttings ash for removing cr (vi) contaminants: adsorption properties, kinetics and mechanism. *J. Environ. Chem. Eng.* **2020**, *8*, No. 104474.
(41) Liu, H.; Li, J.; Zhao, M.; Li, Y.; Chen, Y. Remediation of oil-based drill cuttings using low-temperature thermal desorption: performance and kinetics modeling. *Chemosphere* **2019**, *235*, 1081−1088.
(42) Chen, D.; Zhuang, X.; Gan, Z.; Cen, K.; Ba, Y.; Jia, D. Co-pyrolysis of light bio-oil leached bamboo and heavy bio-oil: effects of mass ratio, pyrolysis temperature, and residence time on the biochar. *Chem. Eng. J.* **2022**, *437*, No. 135253.
(43) Hu, Y.; Xia, Y.; Di Maio, F.; Yu, F.; Yu, W. Investigation of polycyclic aromatic hydrocarbons (pahs) formed in three-phase products from the pyrolysis of various wastewater sewage sludge. *J. Hazard. Mater.* **2020**, *389*, No. 122045.

https://doi.org/10.1021/acsomega.2c07379
ACS Omega 2023, 8, 13593−13604